


# LRIG2 promotes glioblastoma progression by modulating innate antitumor immunity through macrophage infiltration and polarization

Jinyang Hu,<sup>1,2</sup> Feng Dong ,<sup>3,4</sup> You He,<sup>3</sup> Xianyou Xia,<sup>3</sup> Fangling Cheng,<sup>1</sup> Sui Chen,<sup>1</sup> Xiaoshuang Hou,<sup>1</sup> Po Zhang,<sup>1</sup> Guohao Liu,<sup>1</sup> Ying Li,<sup>5</sup> Qian Gao,<sup>6,7</sup> Minhai Dong,<sup>1</sup> Ting Li,<sup>3</sup> Wei Li,<sup>8</sup> Qungen Xiao,<sup>1</sup> Xiaopeng Li,<sup>1</sup> Xingjiang Yu,<sup>9</sup> Guifa Xi,<sup>10,11</sup> Dongsheng Guo,<sup>1</sup> Xudong Wu,<sup>3,4</sup> Baofeng Wang<sup>1</sup>

**To cite:** Hu J, Dong F, He Y, *et al.* LRIG2 promotes glioblastoma progression by modulating innate antitumor immunity through macrophage infiltration and polarization. *Journal for ImmunoTherapy of Cancer* 2022;**10**:e004452. doi:10.1136/jitc-2021-004452

► Additional supplemental material is published online only. To view, please visit the journal online (<http://dx.doi.org/10.1136/jitc-2021-004452>).

JH and FD are joint first authors.

Accepted 10 August 2022

## ABSTRACT

**Background** Glioblastoma (GBM) is the most common malignant brain tumor with poor clinical outcomes. Immunotherapy has recently been an attractive and promising treatment of extracranial malignancies, however, most of clinical trials for GBM immunotherapy failed due to predominant accumulation of tumor-associated microglia/macrophages (TAMs).

**Results** High level of LRIG2/soluble LRIG2 (sLRIG2) expression activates immune-related signaling pathways, which are associated with poor prognosis in GBM patients. LRIG2/sLRIG2 promotes CD47 expression and facilitates TAM recruitment. Blockade of CD47–SIRP $\alpha$  interactions and inhibition of sLRIG2 secretion synergistically suppress GBM progression in an orthotopic murine GBM model.

**Conclusions** GBM cells with high level LRIG2 escape the phagocytosis by TAM via the CD47–SIRP $\alpha$  axis, highlighting a necessity for an early stage of clinical trial targeting LRIG2 and CD47–SIRP $\alpha$  as a novel treatment for patients with GBM.

## BACKGROUND

Glioblastomas (GBM) are the most common malignant brain tumors in adults with average survival less than 2 years, despite aggressive surgical resection adjuvant with radiotherapy and chemotherapy or other novel treatments, such as tumor-treating fields.<sup>1 2</sup> The tumor microenvironment (TME) is an important component directly related to patient prognosis.<sup>3</sup> Emerging evidence demonstrates that infiltrating immune cells play a crucial role in immune evasion and immunotherapeutic resistance in GBM.<sup>4 5</sup> Thus, mechanistic understanding of the infiltration and activities of immunosuppressive cells is expected to identify novel potential therapeutic targets for improving therapeutic efficacy and ultimately clinical outcomes.

Immune cells in GBM tumor-associated microglia and macrophages (TAMs) are

## KEY MESSAGES

⇒ The predominant accumulation of tumor-associated microglia/macrophages (TAMs) results in the limited success of these strategies in glioblastoma (GBM). In this study, we demonstrate that sLRIG2 functions as a potential chemoattractant to recruit macrophages and maintain them in an M2-like behavior, which expresses SIRP $\alpha$ . Our study provides sLRIG2 as a potential prognosis biomarker of response to antitumor immune therapy.

## SIGNIFICANCE

⇒ GBM is the most common malignant brain tumor with poor prognosis, partially due to the complex tumor microenvironment (TME). Mechanistic understanding of the infiltration and activity of immunosuppressive cells in the TME is expected to provide potential and promising therapy strategies. Here, we demonstrate that GBM-secreted sLRIG2 functionalizes as a potential chemoattractant for recruiting macrophages and maintaining the M2 subtype of TAMs. High LRIG2 level in GBM cells increases CD47 abundance. Phagocytic activity of TAMs is suppressed via the CD47–SIRP $\alpha$  axis, which results in the immune escape of GBM cells. Downregulation of LRIG2 or inhibition of sLRIG2 secretion and synergistical blockade of CD47–SIRP $\alpha$  interactions suppress GBM progression. All together, these results suggest the necessity for an early stage of clinical trial targeting LRIG2 and CD47–SIRP $\alpha$  as a novel treatment for patients with GBM.

the main subsets of the microenvironment. Majority (~85%) of TAMs are bone marrow-derived infiltrating macrophages and monocytes. TAMs interact with TME, which are gradually educated to exert immunosuppressive functions through M1-like and M2-like macrophage polarization. M1-like macrophage polarization exhibits anticancer activity by releasing inflammatory cytokines and



© Author(s) (or their employer(s)) 2022. Re-use permitted under CC BY-NC. No commercial re-use. See rights and permissions. Published by BMJ.

For numbered affiliations see end of article.

## Correspondence to

Dr Baofeng Wang;  
wbf620@163.com

Dr Xudong Wu;  
wuxudong@tmu.edu.cn

stimulating naïve T cells to induce cytotoxic response.<sup>6</sup> Macrophage polarization to the M2 subtype promotes tumor growth by secreting inhibitory cytokines and expressing T cell immune checkpoint ligands, thereby suppressing T cell functions.<sup>7,8</sup> Inhibiting recruitment of the bone marrow-derived infiltrating macrophages/monocytes to the GBM microenvironment, or repolarizing M2-like TAMs to the M1 phenotype alleviates GBM progression.<sup>6,9,10</sup> Notably, phagocytosis is an instinct of macrophages, which is lost in TAMs.<sup>11</sup> Among the current models, CD47–SIRP $\alpha$  axis is an essential phagocytosis checkpoints in cancers. CD47 binds to the NH<sub>2</sub>-terminal V-like domain of SIRP $\alpha$  on the TAM to suppress phagocytosis, which causes immune evasion of cancer cells.<sup>11,12</sup> Thus, reactivating TAMs phagocytosis is an attractive therapeutic strategy.

The human leucine-rich repeats and immunoglobulin-like domains (LRIG) gene family, including LRIG1–3, was originally identified as novel negative regulators of the epidermal growth factor receptor (EGFR) signaling pathway. Their encoded proteins share similar molecular structures with distinct functions.<sup>13</sup> LRIG1 and LRIG3 inhibit glioma progression through negative feedback regulation of tyrosine kinase receptors (RTKs).<sup>14</sup> However, LRIG2 overexpression promoted glioma progression by activating RTKs,<sup>15</sup> which mediate immune-related signaling pathways linked to the immunosuppressive TME.<sup>16–19</sup> Knocking out LRIG2 suppresses glioma formation and progression.<sup>20</sup> The extracellular domain of LRIG2 can be cleaved and shed from the cell membrane and secreted into the glioma microenvironment.<sup>21–24</sup> sLRIG2 has similar functions to LRIG2.<sup>22</sup> Therefore, we hypothesized that LRIG2 or sLRIG2 reconfigures the TME to facilitate glioma development.

Here, we showed that LRIG2 induces TAM recruitment through sLRIG2 in GBM. LRIG2 inhibits TAM phagocytosis of GBM cells via the anti-phagocytosis CD47–SIRP $\alpha$  axis, which facilitate immune escape. We also demonstrate that blocking CD47–SIRP $\alpha$  interactions decreases LRIG2 and inhibits sLRIG2 secretion thus suppressing GBM progression.

## MATERIALS AND METHODS

### In silico bioinformatic data analysis

RNA-seq data of glioma samples and their clinicopathological information were analyzed from the dataset (<http://gliovis.bioinfo.cnio.es/>), which contain the Cancer Genome Atlas (TCGA) and the Chinese Glioma Genome Atlas (CGGA) datasets. Kaplan–Meier survival analysis was utilized to assess the correlation between infiltration levels of immune cell subsets and overall survival (OS) of glioma patients. For gene set functional enrichment analysis, the LRIG family members-related gene sets in glioma were obtained from GlioVis (<http://gliovis.bioinfo.cnio.es/>) portal and further analyzed with GO or Kyoto Encyclopedia of Genes and Genomes (KEGG) to evaluate the LRIG-related molecular functions and signaling

pathways.<sup>25</sup> The single-cell sequence data presented in this study was obtained and analyzed with online portal of Single Cell Expression Atlas (SCEA) (<https://www.ebi.ac.uk/gxa/sc/home>).<sup>26</sup> Two single-cell sequence datasets (GSE131928, GSE135437) were selected to evaluate distribution and infiltration level of immune cells, the correlation between infiltration level of immune cells and LRIG family members' expression level were calculated and plotted.

### Cell culture

U87, GL261 and RAW264.7 cells and THP-1 monocytes were purchased from the American Type Culture Collection (Manassas, USA). The human GBM cell line U87, mouse GBM cell line GL261, and mouse macrophage RAW264.7 were cultured in Dulbecco's modified Eagle's medium (DMEM). TPC1115 were obtained from fresh surgical specimens of human primary GBMs and cultured as either monolayer or tumor spheres in DMEM/F12 medium supplemented with N2, B27 (Gibco), 20 ng/mL human fibroblast growth factor-basic (Sino Biological, Beijing, China), 20 ng/mL EGF-basic (EGF, Sino Biological, Beijing, China).<sup>27</sup> THP-1 monocytes were cultured in RPMI 1640 medium (RPMI). All cell lines were cultured in indicated medium supplemented with 10% fetal bovine serum and 1:100 antibiotic-antimycotic (Gibco) and maintained in the humid incubator with 5% CO<sub>2</sub> at 37°C. For differentiation of monocytes to macrophages, THP-1 monocytes were stimulated with serum-free 1640 medium containing 100 ng/mL PMA (Sigma) for 24 hours. All cells were mycoplasma-free detected by PCR.

### Bone marrow-derived macrophages

Mouse bone marrow-derived myeloid precursor cells were harvested from C57BL/6 mice (6–8 weeks old) femurs by syringe and needle. Red blood cells were depleted by ACK lysing buffer. The remaining cells were washed once by PBS and suspended in DMEM containing 20% FCS and 20 ng/mL murine M-CSF (Macrophage Colony Stimulating Factor; Peprotech, Catalog# 315-02) in a 100 mm Petri dish (one femur cells per dish) in an incubator (37°C, 5% CO<sub>2</sub>). Half of the medium was replaced with fresh medium in 3 days.<sup>28</sup>

### Establishment of cell lines with LRIG2 overexpression and knockdown

GBM cells with stable expressions of the full-length LRIG2 or the ectodomain of LRIG2 were established as described previously.<sup>15</sup> To construct LRIG2 stable knockdown GBM cell lines, two shRNAs specifically against human or mouse LRIG2 were designed. The shRNA oligos were annealed and ligated into digested pLKO.1 TRC vector according to the procedure recommended by Addgene (RRID:52920). The constructs were verified by sequencing and co-transfected into 293T cells with VSVG (enveloping) and PAX8 (packaging) plasmid for lentivirus packaging. Virus supernatants were harvested in 48 hours to infect GBM cells at 70% confluence. The

transduced cells were then selected with 2 µg/mL puromycin. The sequences of oligos were listed in online supplemental table 1.

### Purification of GST-sLRIG2 fusion protein

Human sLRIG2 cDNA was amplified and introduced into the vector pGEX-6p-1 (Invitrogen) according to the protocol provided by the manufacturer and verified by sequencing. The primer sequences are listed in online supplemental table 1. The validated plasmid was transferred into *Escherichia coli* strain BL21 and cultured at 37°C in LB media until the optical density at 600 nm reached 0.6. Then 0.22 mM isopropyl-β-D-thiogalactopyranoside was added to induce protein expression at 20°C. The bacteria were harvested in 8 hours, followed by resuspending in 40 mL Bacterial lysate buffer supplemented with protease inhibitors. After ultrasonic crushing, the suspension was filtered by a 0.45 µm Millex filter (Millipore, USA), and the fusion protein was purified with Glutathione sepharose 4B (GE Healthcare; 17-0756-01; 1:1000) and eluted by reduced glutathione (GSH). Finally, the GST-sLRIG2 recombinant protein was concentrated, and the protein concentration was measured.

### siRNA transfection

Small interfering RNA (siRNA) targeting ADAM17, SIRPα, c-Jun and negative control siRNAs (siNC) were purchased from (RIBOBIO, China). Cells were transfected with siRNA using Lipofectamine 3000 Reagent (Invitrogen) following the manufacturer's protocol. The siRNA sequences are listed in online supplemental table 1.

### Detection and elimination of sLRIG2 in the conditioned medium

As described previously,<sup>22</sup> the conditioned medium (CM) was harvested and filtered with a 0.45 µm Millex filter (Millipore). The supernatant was then concentrated by Amicon Ultra-4 10 K centrifugal filter devices (Millipore) spinning at 4000 rpm for 20 min (min). Anti-Flag monoclonal antibody was employed to detect the Flag-tagged sLRIG2. And the anti-Flag M2 Affinity Gel (Sigma A2220) was added in succession to eliminate the sLRIG2 in the conditional medium according to the manufacturer's protocol.

### Immunohistochemistry and HE staining

Immunohistochemistry (IHC) and HE staining were performed as previously described.<sup>27</sup> The corresponding primary antibodies were used for human clinical glioma tissue microarray: anti-LRIG2 (4 µg/mL, RD, MAB19411), anti-CD68 (1:1000, Sigma, HPA048982), anti-CD4 (1:500, Abcam, ab133616), anti-CD8 (1:200, CST, #85336), anti-FOXP3 (1:100, Abcam, ab20034), anti-CD206 (1 µg/mL, Abcam, ab64693), anti-CD47 (1 µg/mL, Abcam, ab175388), anti-c-Jun (1:100, CST, #9165), anti-c-Jun (phospho S63) (1:100, Abcam, ab32385); for mouse glioma tissue: anti-LRIG2 (4 µg/mL, RD, MAB19411), anti-CD68 (1:200, Abcam, ab31630), anti-CD4 (1:100,

CST, #25229), anti-CD8 (1:400, CST, 98941), anti-FOXP3 (1:100, CST, 12653), anti-CD206 (1 µg/mL, Abcam, ab64693), anti-c-Jun (1:100, CST, 9165), anti-c-Jun (phospho S63) (1:100, Abcam, ab32385). The histochemistry score (H-SCORE =  $\sum (PI \times I) = (\text{percentage of cells of weak intensity} \times 1) + (\text{percentage of cells of moderate intensity} \times 2) + (\text{percentage of cells of strong intensity} \times 3)$ ) was employed to estimate the expression level of target protein.

### RT-qPCR

Total RNA was extracted by Trizol (Invitrogen, USA). Equivalent mRNA from each group was reversely transcribed into cDNA using Reverse Transcription Reagents Kit (Thermo Fisher) and amplified by SYBR Green Master Mix (Thermo) on LightCycler 480 SYBR Green I Master (Roche). RPO was employed as the reference gene for all RT-qPCR studies, and the  $\Delta\Delta C_t$  method was performed for quantification analysis. The primer sequences are listed in online supplemental table 1.

### Western blot

Western blot (WB) was performed as previously described.<sup>29</sup> Briefly, cells were harvested and lysed in RIPA buffer supplemented with protease and phosphatase inhibitor cocktails (1%, Sigma-Aldrich) on ice, followed by centrifugation and denaturation. The proteins were separated through SDS polyacrylamide gel electrophoresis and transferred to PVDF membranes. After being blocked in 5% BSA for 1 hour at room temperature, the membranes were incubated with primary antibodies at 4°C overnight and secondary antibodies at room temperature for 1 hour. Then electrochemiluminescence determination (PerkinElmer) was employed to detect the protein levels. Primary antibodies used were as followed: LRIG2 (1:500, Abcam, ab121472), sLRIG2 (1:750, Abcam, ab157492), ADAM17 (1:750, PAB30220), FLAG (1:1000, Sigma, F1804), CD47 (1:1000, Abcam, ab175388), c-Jun (1:1000, CST, #9165), c-Jun (phospho S63) (1:1000, Abcam, ab32385), anti-GAPDH (1:20000, Abclonal, AC002, RRID:AB\_2736879), β-Actin (1:10000, Abclonal, AC026), anti-Albumin (1:1000, Abclonal, A0353). And Direct-load Color Prestained Protein Marker (M221, GenStar) was used in all WB assays.

### Migration assay

Macrophages ( $2 \times 10^5$  for RAW264.7/bone marrow-derived macrophages (BMDMs) and  $5 \times 10^5$  for THP-1 macrophages) were seeded onto 24-well Transwell inserts (5.0 µm) with a serum-free culture medium. Conditioned media was added to the lower chambers. After 48 hours, the migrated macrophages were fixed with methanol and stained with crystal violet (0.05%, Sigma). Cells were then counted per field of view under the microscope.

### In vitro phagocytosis assay

For the in vitro phagocytic assays, we labeled GL261 cells with GFP (GL261-GFP), RAW264.7 with mCherry (RAW264.7-mCherry).  $6 \times 10^5$  RAW264.7-mCherry

macrophages were seeded into the six-well tissue-culture plate in 2 mL fresh medium complemented with 100 ng/mL phorbol 12-myristate 13-acetate (PMA, Sigma-Aldrich). After being cultured for 24 hours,  $3 \times 10^5$  GL261-GFP cells were mixedly cultured with RAW264.7-mCherry for 48 hours. Then wells were washed repeatedly to remove non-phagocytosed cells and then imaged with an inverted microscope (OLYMPUS IX71). The number of macrophages that had phagocytosed GBM cells per 100 macrophages was calculated as the phagocytic index. In vitro phagocytosis assay was also analyzed by flow cytometry.<sup>30,31</sup> GL261 and U87 were labeled with GFP, RAW264.7/BMDMs were identified by APC/PE anti-mouse F4/80 (BioLegend) and THP-1 macrophages were identified by APC anti-human CD11b (BioLegend).  $1 \times 10^6$  adherent macrophages were seeded into the 6-well tissue-culture plate in 2 mL fresh medium,  $5 \times 10^5$  GFP-labeled GBM cells were co-cultured with macrophage for 48 hours. Then wells were washed to remove non-phagocytosed cells following flow cytometry analysis. Phagocytosis was measured as the number of CD11b<sup>+</sup>/F4/80<sup>+</sup>GFP<sup>+</sup> macrophages, quantified as a percentage of the total CD11b<sup>+</sup>/F4/80<sup>+</sup> macrophages.

To capture the phagocytosis, the live-cell workstation (Cytation5, BioTek Instruments) was employed to photograph the co-incubated cells (GBM cell and macrophages as described above) cultured in a 37°C incubator at 5 min intervals using optimized parameters according to the instructions.

### Tumor dissociation and flow cytometry

Samples were enzymolysed in 1640 media supplemented with 2% BSA, collagenase hyaluronidase (Stem Cell Technologies) and DNase (Worthington). Tissue was rotated on a Rotating Micro-Tube Mixer for 1 hour at 37°C until the single-cell suspension was obtained. After being filtered with a 70 µm filter and washed with PBS, the single-cell suspension was stained with fluorescent antibodies (CD45-FITC, CD11b-APC-cy7, CD206-APC, F4/80-PE, TMEM119-PE, CD11c-Pecy7) for flow cytometry analyses.<sup>32</sup>

### Luciferase reporter assay

The CD47 promoter or mutant variant was amplified by PCR and cloned into the pGL4.23 (luc2/minP) Vector (Promega, E841A) at NheI and HindIII sites. Sequences of CD47 promoter and mutant promoters were listed in online supplemental table 1. For dual-luciferase reporter assays, HEK-293T cells were seeded into a 24-well plate and then co-transfected with the pLVX-Tight-LRIG2 or the negative control (pLVX-Tight-CON) (500 ng/well) and the pGL4.23 reporter vector (500 ng/well) by PEI (poly science). After 48 hours of transfection, luciferase activities were detected by the Dual-Luciferase Reporter Assay Kit (Promega) according to the manufacturer's instructions.

### Animal studies

Female C57BL/6 mice (6–8 weeks old) were purchased from Beijing Sibeifu Bioscience (Beijing, China).

$2 \times 10^5$  GL261 cells expressing luciferase were suspended in 2 µL PBS and transplanted into the frontal lobes of brains of Female C57BL/6 mice (6–8 weeks old) by stereotaxic intracranial injection as previously described.<sup>27</sup> Post 7 days and 21 days of implantation, bioluminescence imaging (BLI) (IVIS; Xenogen) was taken to monitor intracranial tumor growth. Mouse anti-CD47 blocking antibody (clone MIAP-301; BioXcell) and TAPI-1 (R11750; rechem-science;) were administered as followed: MIAP-301,<sup>33,34</sup> (16 mg per kg) was injected intraperitoneally every other day while TAPI-1 (50 mg per kg) injected intraperitoneally 5 days per week. Mice survival was recorded and analyzed accordingly.

### Statistical analysis

Statistics were performed using software GraphPad Prism V.7.0 (GraphPad Prism Software, San Diego, California, USA). A two-tailed unpaired Student's t-test and Pearson's correlation test were used as appropriate. For survival comparison, a log-rank test was used. Data that match the normal distribution and homogeneity of variance test (Shapiro-Wilk normality test:  $p > 0.05$ ; Brown-Forsythe test:  $p > 0.05$ ) were analyzed by the Student's t-test for two-group comparisons. Statistical analysis by one-way analysis of variance with Bonferroni correction for multiple comparisons. Otherwise, non-parametric tests (Kruskal-Wallis test with Dunnett's correction) were used for multiple comparisons. Error bars indicate the mean ± SD. P values were expressed as follows: \* $p < 0.05$ , \*\* $p < 0.01$ , \*\*\* $p < 0.001$ , and \*\*\*\* $p < 0.0001$ .

## RESULTS

### High LRIG2 is correlated with higher glioma TAM density and shorter survival

To investigate the role of LRIG gene family in glioma immune microenvironment, we analyzed the levels of LRIG1-3 in the SCEA and GEO dataset (GSE131928; GSE135437). The results showed that LRIG2 level, compare to those of LRIG1 and LRIG3, were significantly increased in both tumor and immune cells, especially in mono/macrophages (figure 1A and online supplemental figure S1A). To further investigate LRIG2 associated genes in GBM, we further analyzed TCGA datasets, the KEGG results demonstrate that LRIG2-related gene sets were enriched in immune-related pathways (eg, cytokine–cytokine receptor interaction) and GO analysis indicated that LRIG2 is functionally correlated with leukocyte cell-cell adhesion, leukocyte aggregation (figure 1B and online supplemental figure S1B).

To further elucidate whether specific immune cell subsets are associated with high level of LRIG2 in the glioma immune microenvironment, tissue microarray with 88 glioma tumor specimens were prepared for IHC. The results showed high LRIG2-expressing gliomas also exhibited high expression levels of CD68 and CD206 (figure 1C,D and online supplemental figure S1C, D). We further investigated patients' survival in the CGGA

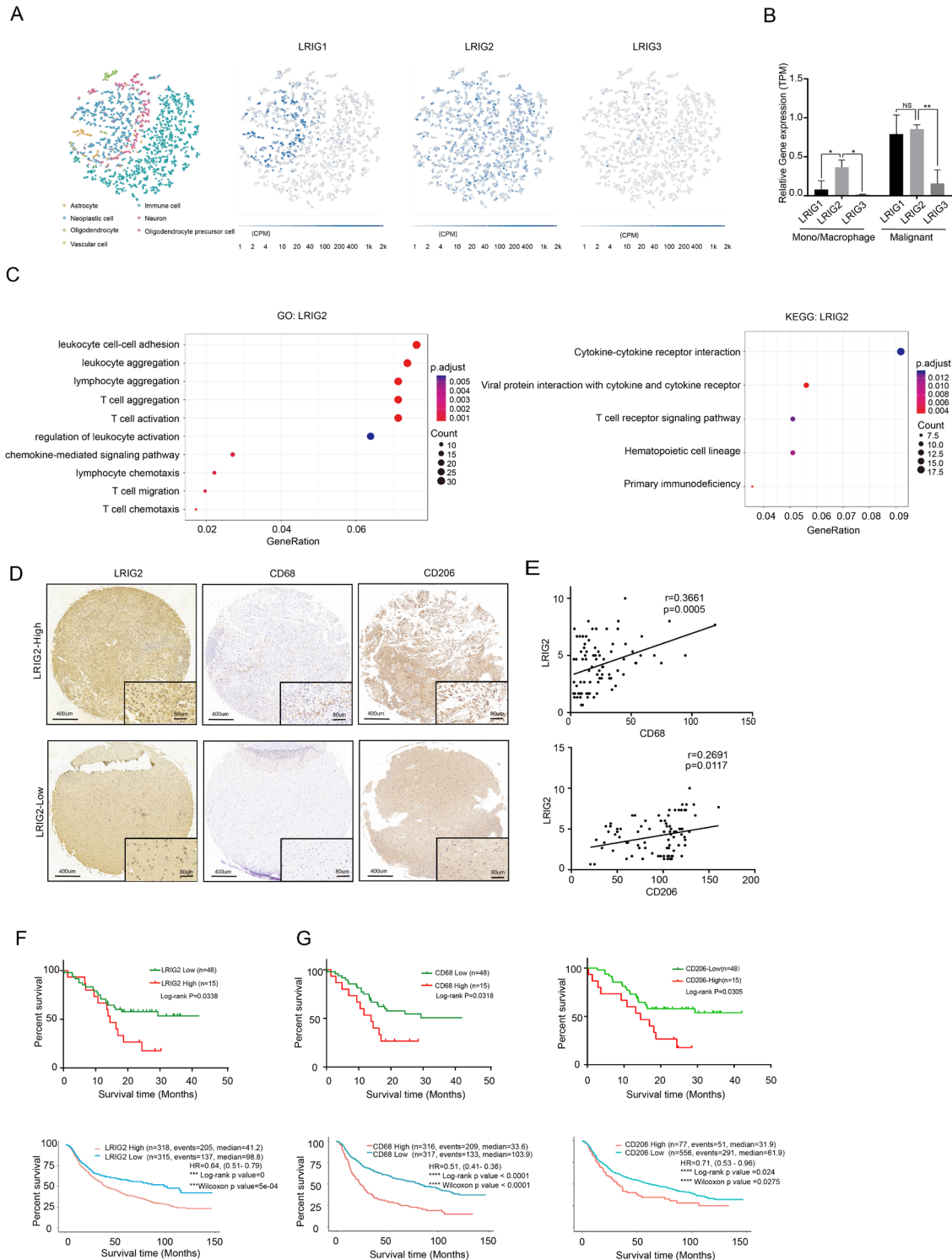


**Figure 1** High LRIG2 is correlated with higher glioma TAM density and shorter survival. LRIG family members' expression level in glioma cells and the infiltration of immune cells from the SCEA datasets \* $P < 0.05$ , \*\* $P < 0.01$ . (A) and GEO datasets (GSE131928; GSE135437) (B). Unpaired Student's t-test. Error bar=SD. (C) GO and KEGG pathway enrichment analysis of LRIG2-related gene sets in glioma from the TCGA datasets. (D) Representative IHC images of the infiltration of immune cell subsets in LRIG2 high ( $H\text{-SCORE} \geq 6$ ) and low expression ( $H\text{-SCORE} < 6$ ) tumors. Top panel: scale bar, 400  $\mu\text{m}$ . Bottom panel: scale bar, 80  $\mu\text{m}$ . (E) Correlation analysis between the protein expression (D) of LRIG2 and the TAM marker CD68 and CD206 in clinical glioma tissue microarray ( $n=88$ , H-SCORE). Pearson's correlation test. (F) Kaplan-Meier survival curves for correlation between mRNA and protein expression of LRIG2 and survival of glioma patients in the CGGA dataset and clinical glioma tissue microarray. Log-rank test. (G) Kaplan-Meier survival analysis for the correlation between infiltration degree of immune cell subsets in glioma microenvironment and survival of glioma patients in the CGGA dataset and clinical glioma tissue microarray, log-rank test. CGGA, Chinese Glioma Genome Atlas; KEGG, Kyoto Encyclopedia of Genes and Genomes; ns, not significant; TAM, tumor-associated microglia/macrophage; TCGA, The Cancer Genome Atlas.

database and clinical tumor samples based on LRIG2, CD68, CD206 and CD8 expression levels, The results showed that survival duration was shorter in patients with higher LRIG2 expression and TAM infiltration. The patient survival varies depending on CD8<sup>+</sup> T cell infiltration detected by protein or mRNA expression (figure 1E,F, and online supplemental figure S1E). Taken together, these results suggest that high LRIG2 correlates with TAM infiltration in glioma tumor specimens and is potentially associated with poor prognosis in patients with GBM.

### LRIG2 promotes TAM recruitment and M2-like polarization in GBM

To further elucidate the roles of LRIG2 in the glioma microenvironment in vivo, we generated LRIG2 knock-down GL261 cells using two sets of short hairpin-RNAs (shRNAs) against LRIG2 (shLRIG2-1 and shLRIG2-2) (online supplemental figure S2A), which were documented with luciferase using lentivirus transduction before intracranial injection. The results indicated that LRIG2 downregulation resulted in a significant tumor volume reduction as evaluated by the BLI (figure 2A,B). Mice-bearing tumors derived from LRIG2-depleted GL261 cells showed significantly prolonged survival (figure 2C). Moreover, IHC analysis showed that the numbers of local CD68-positive TAMs and CD206-positive TAM were significantly lower in the LRIG2-deficient tumors versus the tumors in the control group (figure 2D,E). Further analysis of TAM density in the tumor mass by flow cytometry revealed that the infiltration of tumor-associated macrophages (CD45<sup>+</sup>CD11b<sup>+</sup>F4/80<sup>+</sup>) possess a higher proportion than TAM (CD45<sup>+</sup>CD11b<sup>+</sup>TMEM119<sup>+</sup>) in GL261 cells derived tumors (figure 2F). CD45<sup>+</sup>CD11b<sup>+</sup>F4/80<sup>+</sup> macrophages and CD45<sup>+</sup>CD11b<sup>+</sup>F4/80<sup>+</sup> CD206<sup>+</sup> M2-like TAM density were dramatically reduced. M1-like TAM (CD45<sup>+</sup>CD11b<sup>+</sup>F4/80<sup>+</sup>CD11c<sup>+</sup>) were significantly increased in the LRIG2 knockdown group in vivo (figure 2G). These findings demonstrate that silencing LRIG2 in GBM reduces M2-like tumor-associated macrophages infiltration and prolongs the survival for the mice-bearing tumors with shLRIG2.

To further investigate whether macrophage chemotaxis and polarization were mediated by LRIG2 in vitro, we conducted a series of migration assays. The results showed that CM from LRIG2 and sLRIG2 overexpressed cells attracted more macrophages than those from the control groups. In contrast, fewer macrophages were attracted to CM from LRIG2 depleted cells. Interestingly, sLRIG2 overexpressed cells derived supernatant significantly increased macrophage migration compared with the supernatant from LRIG2 overexpressed cells (figure 2H and online supplemental figure S2C). The results showed that the macrophage migration was attenuated when FLAG-sLRIG2 was cleared from the supernatant by using anti-FLAG M2 beads (online supplemental figure S2D, E). Moreover, GST-sLRIG2 recombinant fusion protein, which was synthesized and purified in *E. coli* (online

supplemental figure S2F), enhances the proliferation of GBM cells in vitro (online supplemental figure S2G). In addition, more GST-sLRIG2 treated macrophages in serum-free medium migrated from the upper chamber to the lower chamber compared with the GST treatment (figure 2J). These results indicate that sLRIG2 serves as a macrophage chemoattractant in vitro.

M2-like macrophages are more chemotactic and beneficial to glioma progression than M1-like macrophages.<sup>5,35</sup> sLRIG2 promotes TAM recruitment. We hypothesized that sLRIG2 may induces M2 polarization in vitro, which was supported by (1) the supernatant from sLRIG2 overexpressed cells downregulates the mRNA levels of M1 markers (IL-1 $\beta$ , TNF- $\alpha$ , il-1 $\beta$ , and TNF- $\alpha$ ) and upregulated the expression levels of M2 markers (TGM2, SIRP $\alpha$ , CD206, VEGF, Tgm2, Sirp $\alpha$ , Cd206, Mgl1, and Mgl2) (figure 2J) and (2) the expression levels of TGM2, SIRP $\alpha$  were remarkably increased as indicated by WB (figure 2K).

### LRIG2 inhibits the macrophage-mediated GBM cell phagocytosis by activating CD47/SIRP $\alpha$ axis

CGGA database and clinical tissue microarray analysis showed that the expression of SIRP $\alpha$  were positively correlated with the ones of receptor CD47 (figure 3A). LRIG2 regulates the expression levels of SIRP $\alpha$ , suggesting LRIG2 might affect macrophage phagocytosis functions through the CD47/SIRP $\alpha$  axis. To this end, we in silico analyzed the CGGA database and Clinical tissue microarray. the results showed that the mRNA and protein expression of LRIG2 and CD47 were positively correlated (online supplemental figure S3A). CD47 reduction was observed in the LRIG2-deficient cells (figure 3B,C), CD47 overexpression was detected in LRIG2 overexpressed cells while SIRP $\alpha$  overexpression was detected in macrophages treated with LRIG2 overexpressed cells derived supernatant (online supplemental figure S3B, D). Interestingly, LRIG2 depleted GBM were more likely to be phagocytized by macrophages than tumor cells in the control group (figure 3D-G).

To further evaluate whether LRIG2-suppressed phagocytosis depends on the CD47-SIRP $\alpha$  axis, we knocked down CD47 in LRIG2-overexpressed cells or depleted SIRP $\alpha$  in macrophages (online supplemental figure S3B, C). In vitro phagocytosis assay showed that LRIG2-overexpressed cells were less likely to be phagocytized by macrophages compared than the cells in the control groups. However, depletion of CD47 in LRIG2-overexpressed cells or SIRP $\alpha$  in macrophages, remarkably enhanced the LRIG2-induced reduction of phagocytosis to the level which is similar to that in the control group (figure 3H-K). The results indicate that LRIG2 attenuates macrophage phagocytic activity via the CD47/SIRP $\alpha$  axis.

### LRIG2 promotes CD47 transcription by c-Jun

c-Jun is an important downstream transcription factor in the RTK signaling pathway<sup>36</sup> to regulate CD47

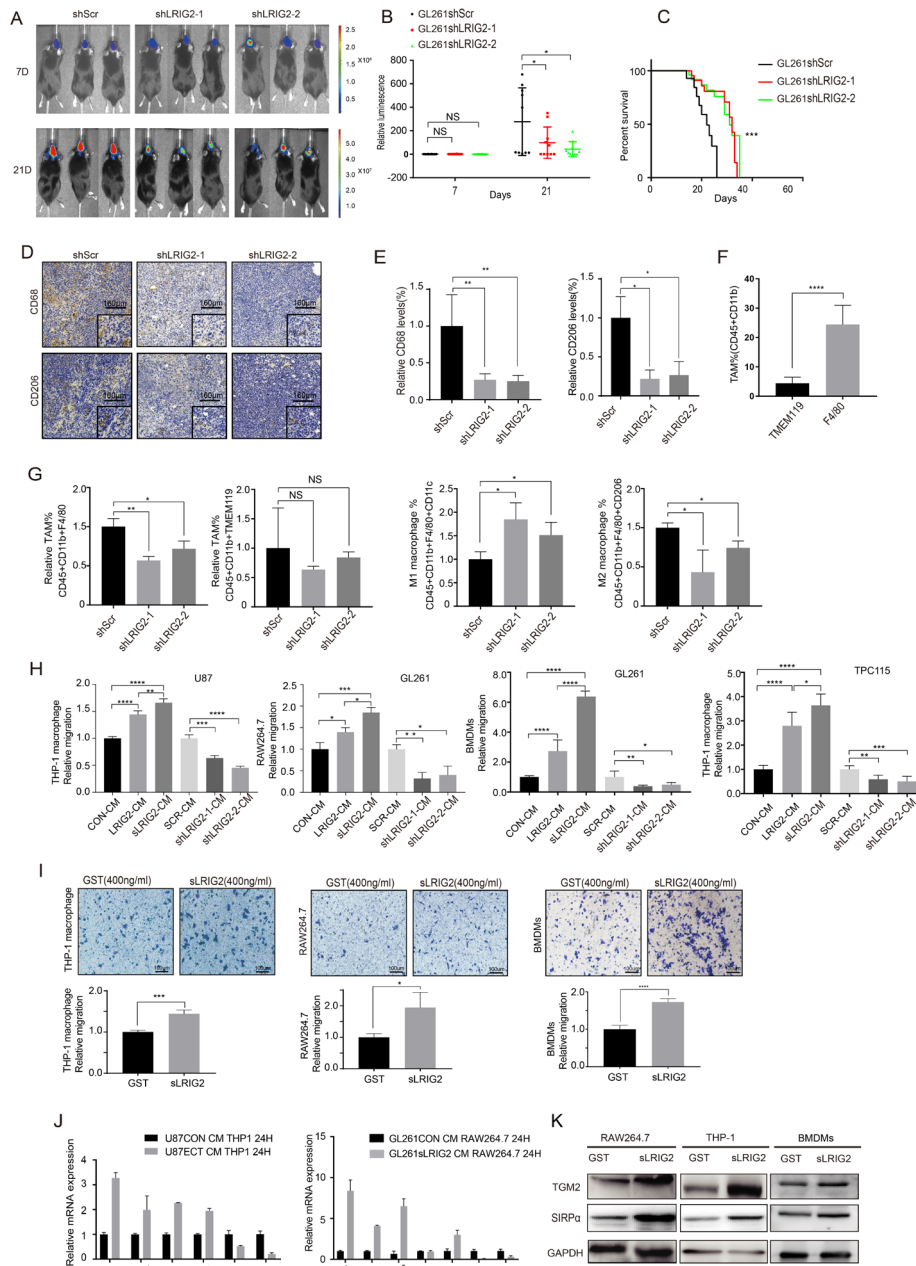


**Figure 2** LIRIG2 promotes TAM recruitment and M2 polarization in GBM. The representative luciferase images (A) and the averages bioluminescence signals of mice after 7 and 21 days from tumor implantation (B) (mean±SD; n=10). The unpaired Student's t-test determined the significance level. \*P<0.05. (C) Kaplan-Meier survival curves for mice intracranially implanted with GL261 cells with or without LIRIG2 knockdown. Kaplan-Meier survival comparison was performed using log-rank test, \*\*\*p<0.001. n=10. (D) Representative IHC images of CD68, CD206 protein levels in control and LIRIG2 knockdown group. Bottom panel: scale bar, 160 μm. (E) Graphic analysis of (figure 2D) indicating that the local CD68 positive cells and CD206 positive cells in tumor section after LIRIG2 knockdown. Unpaired Student's t-test. (F) Graphic analysis showing that the infiltration of tumor-associated macrophages(CD45+CD11b+F4/80+) in GL261 cells derived tumors. (G) Graphic analysis showing that the infiltration of tumor-associated macrophages and M2-like TAM(CD45+CD11b+F4/80+CD206+) in LIRIG2 knockdown GL261 cells derived tumors (mean±SD; n=3). The unpaired Student's t-test determined the significance level, \*p<0.05. (H) Quantification of relative migration macrophages (THP1 macrophages, RAW264.7, BMDMs) towards conditioned media from matched LIRIG2 overexpressed or deficient GBM cells (U87, GL261, TPC115) by migration assays. Scale bar=100 μm. Unpaired Student's t-test. \*\*p<0.01. (I) Representative images and quantification of relative migration of RAW264.7, THP-1 macrophages, and BMDMs treated with GST (400 ng/mL) or GST-sLIRIG2 (400 ng/mL). One-way ANOVA with Bonferroni correction. \*\*\*\*p<0.0001. (J, K) The mRNA and protein expression level of M1 and M2 markers of macrophages treated with GST (400 ng/mL) or sLIRIG2 (400 ng/mL) examined by RT-qPCR (K) and WB analysis (L). Values are expressed as relative expression levels to housekeeping gene RPO. ANOVA, analysis of variance; BMDM, bone marrow-derived macrophages; GBM, glioblastoma; IHC, immunohistochemistry; ns, not significant; TAM, tumor-associated microglia/macrophages; WB, Western blot.

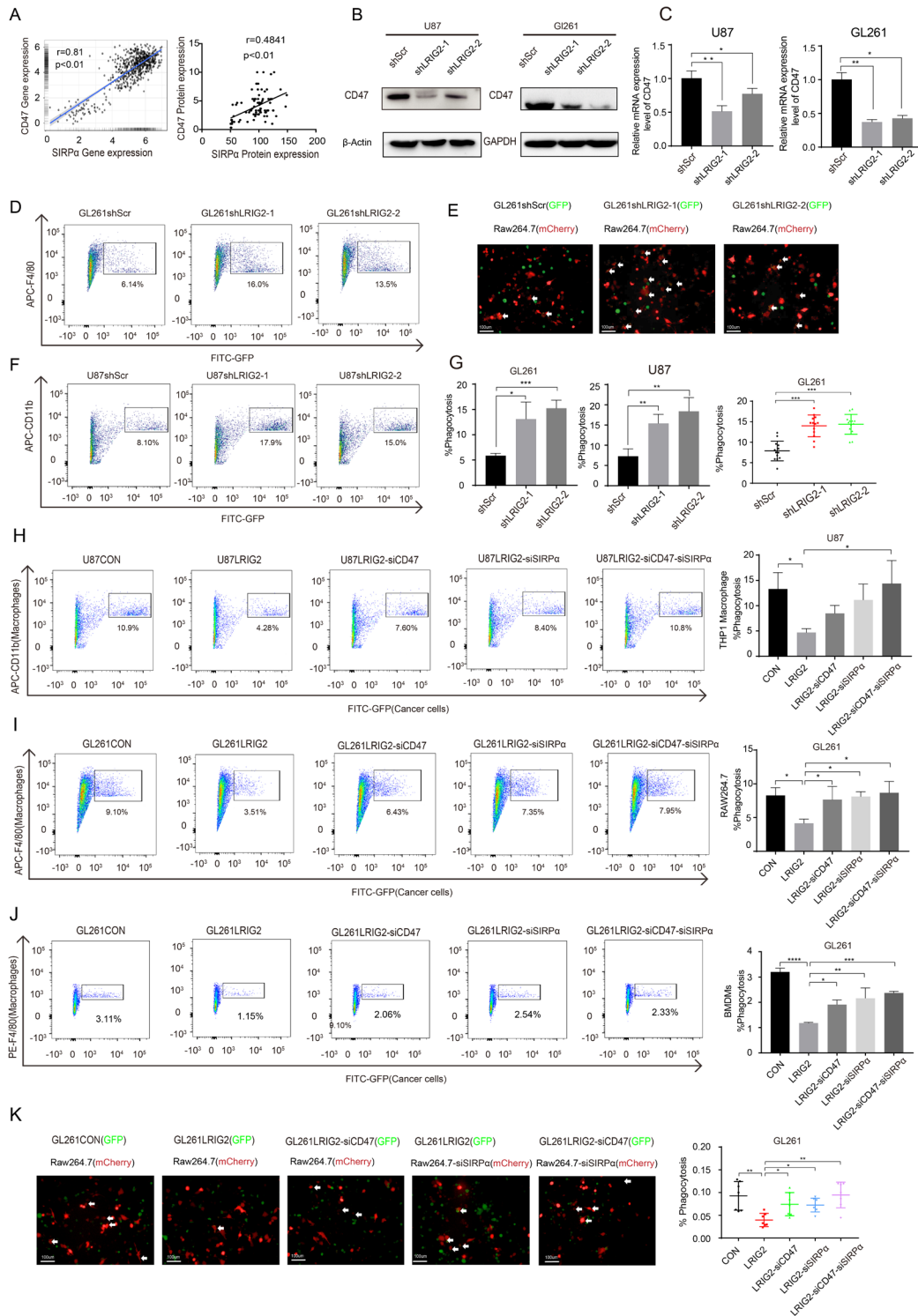


**Figure 3** LRI2 inhibits the macrophage-mediated GBM cell phagocytosis by activating the CD47/SIRP $\alpha$  axis. (A) The correlation analysis between the mRNA and protein expression level of SIRP $\alpha$  and CD47 in the CGA database and clinical glioma tissue microarray. Pearson's correlation test. (B, C) The protein and mRNA expression levels of LRI2 and CD47 in LRI2 knockdown GBM cells and control group determined by WB (B) analysis and RT-qPCR (C). Unpaired Student's t-test. (D–G) Representative images of flow cytometric and graphical analysis of the macrophage-mediated phagocytosis of GBM cells with or without LRI2 knockdown. (mean $\pm$ SD, n=3). Unpaired Student's t-test was used to determine the significance between the two groups, \* $p<0.05$ , \*\* $p<0.01$ . (H–K) In vitro phagocytosis assay analysis of the macrophage-mediated phagocytosis of GL261CON, GL261LRI2, GL261LRI2-siCD47 cells co-cultured with RAW264.7-siNC or RAW264.7-siSIRP $\alpha$ , BMDMs-siNC or BMDMs-siSIRP $\alpha$  and U87CON, U87LRI2, U87LRI2-siCD47 cells co-cultured with THP1-siNC macrophages or THP1-siSIRP $\alpha$  macrophages. n=3, Kruskal-Wallis test with Dunnett's correction (H); one-way ANOVA with Bonferroni correction (I–K) (\* $p<0.05$ , \*\* $p<0.01$ , \*\*\* $p<0.0001$ ). ANOVA, analysis of variance; BMDM, bone marrow-derived macrophage; GBM, glioblastoma; WB, Western blot.



expression in fibroblasts.<sup>37</sup> To verify if it is also true in glioma, we analyzed the CGGA database and clinical tissue microarray, the results showed that the expressions of LRIG2 and CD47 was positively correlated with c-Jun at the mRNA and protein levels (online supplemental Figure S4A–C). Moreover, the IHC of tumor sections showed that the expression levels of c-Jun, p-c-Jun and CD47 were significantly decreased in LRIG2-deficient tumors versus those in the control group (online supplemental figure S4D, E). In contrast, enhanced CD47, c-Jun and p-c-Jun expressions were detected in the LRIG2 overexpressed cell. Downregulation of c-Jun or inhibition of c-Jun phosphorylation significantly inhibited the increased CD47 expression (online supplemental figure S4F).

There are two putative c-Jun-binding sites within the CD47 promoter. To further explore whether c-Jun directly binds to CD47 promoter in glioma, we generated reporter constructs with either wild-type *CD47* promoters or mutants that disrupt the potential binding of c-Jun (online supplemental figure S4G). Overexpression of LRIG2 increased CD47 promoter activity compared with that in the control (online supplemental figure S4H). However, it failed to activate the reporter with mutated c-Jun binding sites. Hence, LRIG2 upregulates CD47 expression by interacting with c-Jun.

### ADAM17 mediates the shedding of the ectodomain of LRIG2 (sLRIG2)

Cell-surface transmembrane proteins are often cleaved and shed into the blood under pathological conditions, making them ideal targets for diagnostic blood markers.<sup>38</sup> Given the extracellular domain of LRIG2 can be shed from the cell membrane and secreted into the glioma microenvironment. A disintegrin and metalloproteinase 17 (ADAM17) sheds sLRIG1 from the full-length LRIG1,<sup>39</sup> and a similar amino acids sequence of the transmembrane between LRIG1 and LRIG2,<sup>13</sup> We propose that a similar mechanism applies to the production of sLRIG2. To this end, we treated LRIG2-overexpressed cells with ADAM17 activator (PMA) and found that PMA increased supernatant sLRIG2 and reduced intracellular LRIG2 (figure 4A). Knocking down ADAM17 in LRIG2 overexpressed cells decreases supernatant sLRIG2 and increases intracellular LRIG2 (figure 4B). Moreover, PMA-induced shedding of sLRIG2 was blocked by an ADAM17 inhibitor (TAPI-1) (figure 4C). Therefore, ADAM17 is indispensable for shedding the ectodomain of LRIG2.

### Targeting LRIG2 expression/secretion synergizes with anti-CD47 in anti-GBM therapeutics

The above findings led us to determine whether targeted LRIG2 and anti-CD47 antibody treatment combined with ADAM17 inhibitors could effectively improve the glioma

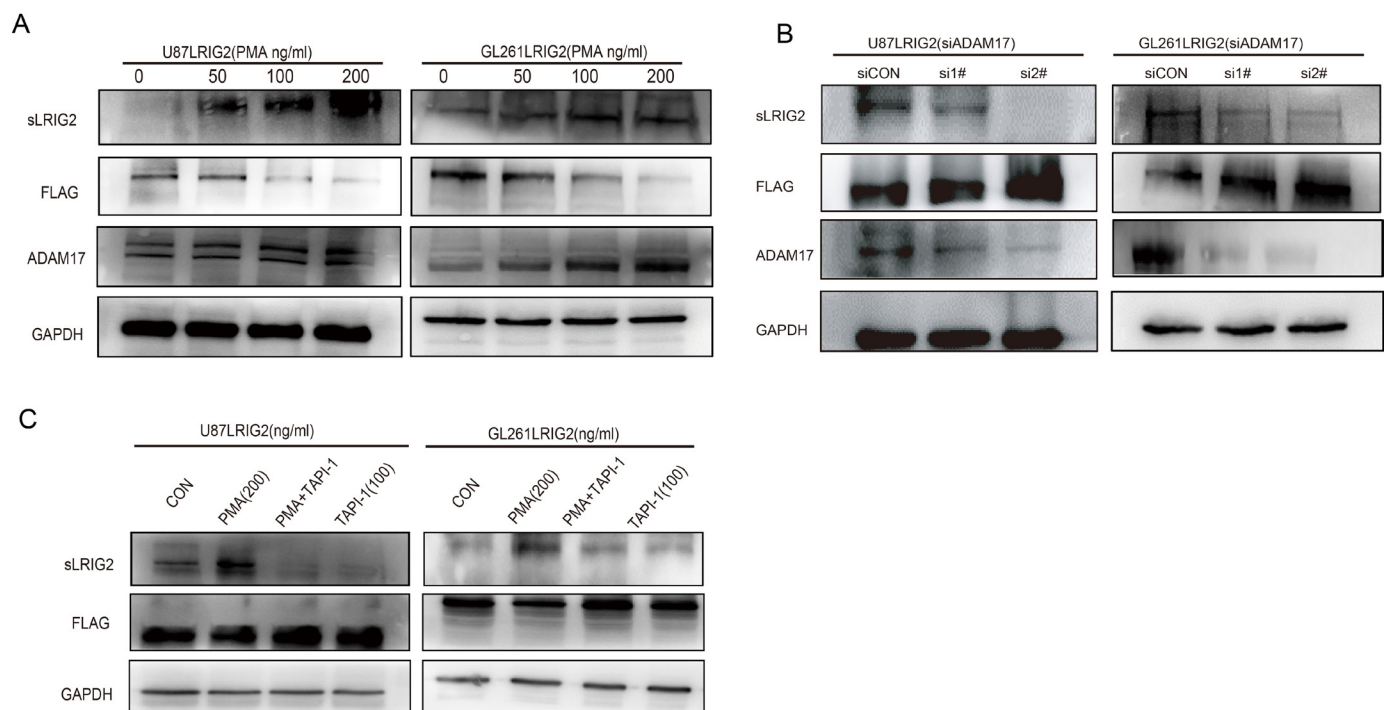


**Figure 4** ADAM17 mediates the shedding of the ectodomain of LRIG2 (sLRIG2) (A) WB analyses the expression of sLRIG2 in the supernatant and FLAG, ADAM17 in the cytoplasm of U87-LRIG2 and GL261-LRIG2 cells treated with four different concentrations of ADAM17's activator (PMA 0 ng/mL, 50 ng/mL, 100 ng/mL, 200 ng/mL). (B) WB analyses the protein expression of sLRIG2 in the supernatant and FLAG and ADAM17 in the intracellular of LRIG2 overexpressed GBM cells transfected with two different siRNA targeting ADAM17. (C) WB analyses the protein expression level of sLRIG2 in the supernatant and FLAG in the intracellular of LRIG2 overexpressed GBM cells treated with ADAM17's activator (PMA 200 ng/mL) or ADAM17's inhibitor (TAPI-1 100 ng/mL) or PMA (200 ng/mL) and TAPI-1 (100 ng/mL). GBM, glioblastoma; WB, Western blot.

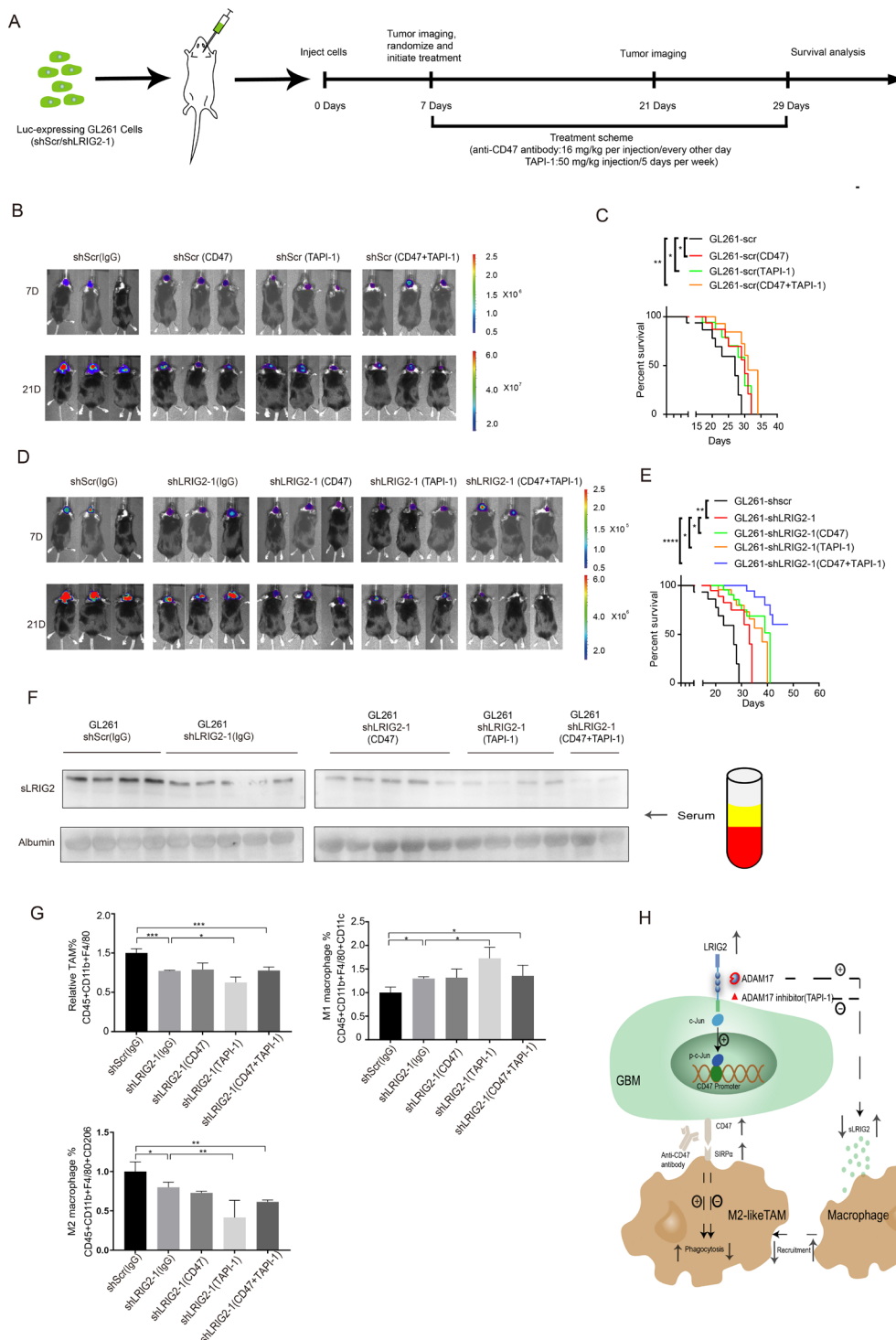


**Figure 5** Targeting LIRG2 expression/secretion synergizes with anti-CD47 in anti-GBM therapeutics. (A) Treatment scheme for evaluating *in vivo* efficacy of targeting LIRG2 combined with anti-CD47 and TAPI-1. (B) and (C) Representative luciferase images of GL261shScr cells (B) or GL261shLRIG2-1 (C) derived tumors in mice treated with IgG control, anti-CD47, TAPI-1, or TAPI-1 and anti-CD47 antibody (n=8). (D, E) Effect of monotherapy and combination anti-CD47 and TAPI-1 on tumor-bearing (GL261shScr cells/GL261shLRIG2-1 cells) mice (n=8/9). Kaplan-Meier survival curves for each treatment group. Significance level was calculated by log-rank analysis. \* $P < 0.05$ , \*\* $p < 0.01$ , \*\*\* $p < 0.001$ . (F) Western blotting of sLRIG2 in the serum of tumor-bearing mice from different groups (GL261shScr-IgG, GL261shLRIG2-1 IgG, GL261shLRIG2-1 anti-CD47, GL261shLRIG2-1 TAPI-1, GL261shLRIG2-1-anti-CD47+TAPI-1). (G) Graphic analysis of M2-like TAM (CD45+CD11b+F4/80+CD206+) and M1-like TAM (CD45+CD11b+F4/80+CD11c+) cells density in the control group (GL261-shScr), LIRG2 knockdown group (GL261shLRIG2-1), LIRG2 knockdown group treated with anti-CD47 antibody (GL261shLRIG2-1 CD47), LIRG2 knockdown group treated with TAPI-1 (GL261shLRIG2-1 TAPI-1), LIRG2 knockdown group treated with anti-CD47 antibody and TAPI-1 (GL261shLRIG2-1 CD47 TAPI-1). (Mean $\pm$ SD; n=4). \* $P < 0.05$ , \*\* $p < 0.01$ , \*\*\* $p < 0.001$ . One-way ANOVA with Bonferroni correction. (H) Proposed schematic of LIRG2 mediates GBM immune escape. ANOVA, analysis of variance; GBM, glioblastoma.

microenvironment and achieve optimized therapeutic effects. After establishing an orthotopic murine GBM model with control and LRIG2-depleted GL261 cells, anti-CD47 and/or TAPI-1 treatment were initiated (figure 5A). The results showed that anti-CD47 antibody/TAPI-1 alone or in combination treatment mildly suppressed tumor progression and achieved a limited survival benefit when LRIG2 was highly expressed (figure 5B,C). On LRIG2 depletion, anti-CD47 or TAPI-1 treatment alone effectively suppressed tumor growth. Moreover, anti-CD47 or TAPI-1 combination treatment remarkably inhibited tumor growth and extended survival in comparison to the untreated group (figure 5D,E).

To further assess the effect of combination therapy on TME in vivo, we analyzed the density of CD45+CD11b+F4/80+TAM, CD45+CD11b+F4/80+CD206+M2-like TAM, CD45+CD11b+F4/80+CD11c+M1-like TAM with Flow Cytometry and CD206+positive TAM with IHC in tumor tissues and the sLRIG2 expression levels in the serum of tumor-bearing mice from different groups. Interestingly, M2-like TAM density in the tumor section and the sLRIG2 expression in serum was significantly decreased in LRIG2-deficient GBM versus those in the control group. Moreover, the M2-like TAM density in the tumor section and the sLRIG2 expression were significantly lower in tumor-bearing mice treated with TAPI-1 than those in the LRIG2 knockdown group (figure 5F,G, online supplemental figure S6A, B). In line with these findings, CM from GL261shLRIG2-1 (TAPI-1) suppresses the chemoattractant effects on RAW264.7 compared with CM from LRIG2-depleted cells (online supplemental figure S5A). Moreover, on treating GL261 shScr and GL261shLRIG2-1 cells with an anti-mouse CD47 mAb, the results showed that LRIG2 deficient cells enhanced macrophage phagocytic activity compared with the control group (online supplemental figure S5B). Overall, these data indicate that LRIG2 depletion, blocking the CD47–SIRP $\alpha$  axis, and inhibiting the secretion of sLRIG2 have therapeutic potential to improve GBM immunotherapy efficacy.

## DISCUSSION

Immune checkpoint therapy has attracted significant attention in recent years. here, we demonstrated that GBM-secreted sLRIG2 functions as a potential chemoattractant to recruit macrophages but not microglial and maintain the M2 subtype of TAMs, via in silico analyzing clinical data, in combination with comprehensive gain-of-function or loss-of-function assays. We also showed that that high LRIG2 expression in GBM cells increases CD47 abundance, which suppresses TAM phagocytic activity via the CD47–SIRP $\alpha$  axis and ultimately results in the immune escape (figure 5H). Accordingly, inhibiting the secretion of sLRIG2 and blockade of CD47–SIRP $\alpha$  interactions synergistically suppresses GBM progression.

ADAM17 is responsible for the protease-driven shedding of more than 70 membrane-tethered cytokines, growth factors, and cell surface receptors,<sup>40</sup> Here, we show ADAM17 could also effectively mediate shedding ectodomain of LRIG2 in GBM cells. TAPI-1, a chemical inhibitor of ADAM17,<sup>3</sup> prevents the release of sLRIG2 into the TME and suppresses macrophages recruitment in vitro. INCB7839, an ADAM10/17 inhibitor, effectively inhibits pediatric high-grade glioma growth by inhibiting ADAM10-mediated cleavage of NLGN3.<sup>3</sup> Which is currently in phase I clinical trials (ClinicalTrials.gov Identifier: NCT04295759). Accordingly, we speculate that it may also inhibit the progression of GBM by inhibiting the release of sLRIG2 mediated by ADAM17. Based on our mechanistic insights, the sLRIG2 abundance in patients' serum may reflect a possible biomarker for the stratification of patients before treatment and a monitoring indicator for the therapeutic efficacy.

We also found that targeting LRIG2 could downregulate CD47 abundance in GBM, CD47 monoclonal antibody could block the CD47–SIRP $\alpha$  axis and inhibit tumor progression,<sup>34,41</sup> however, the antitumor effect of the CD47 antibody alone is limited in GBM.<sup>42</sup> Here, we established a phagocytosis model in vitro and found that targeting LRIG2 to reduces the abundance of CD47 in GBM cells and combination with CD47 antibody can effectively enhance macrophages-mediated phagocytosis. Macrophages are an important source of antigen-presenting cells (APCs). Hence, further investigation is necessary to validate whether LRIG2 depletion improves the antigen presentation efficiency to prime T cells and activates downstream adaptive immune responses, in addition to boosting phagocytosis. Moreover, bispecific antibodies designed for LRIG2 and CD47 may increase therapeutic effects, especially in combined with the ADAM17 inhibitor INCB7839 or TAPI-1.

In summary, here, we addressed the mechanism that LRIG2/sLRIG2 mediates glioma immune escape by manipulating TAMs via the CD47–SIRP $\alpha$  axis, which suggests LRIG2 is not only a potential biomarker for predicting OS and also a promising therapeutic target in patients with GBM. Thus, targeting LRIG2/sLRIG2 adjuvant to traditional or other novel therapy could improve immunotherapeutic efficacy against GBM, highlighting a necessity for an early stage of clinical trial.

## Author affiliations

<sup>1</sup>Department of Neurosurgery, Huazhong University of Science and Technology, Tongji Hospital, Tongji Medical College, Wuhan, Hubei, China

<sup>2</sup>Department of Neurosurgery, The First People's Hospital of Yichang, China Three Gorges University People's Hospital, Yichang, Hubei, China

<sup>3</sup>State Key Laboratory of Experimental Hematology, The Province and Ministry Co-sponsored Collaborative Innovation Center for Medical Epigenetics, Cancer Institute and Hospital, Department of Cell Biology, Tianjin Medical University, Tianjin, China

<sup>4</sup>Department of Neurosurgery, Laboratory of Neuro-Oncology, Tianjin Medical University General Hospital, Tianjin, China

<sup>5</sup>Experimental Medicine Center, Huazhong University of Science and Technology, Tongji Hospital, Tongji Medical College, Wuhan, Hubei, China

<sup>6</sup>Department of Oral and Maxillofacial Surgery, Peking University School of Stomatology, Beijing, China

<sup>7</sup>Central Laboratory, Peking University School of Stomatology, Beijing, China

<sup>8</sup>Tianjin First Central Hospital, Tianjin, China

<sup>9</sup>Department of Histology and Embryology, College of Basic Medicine, Huazhong University of Science and Technology, Wuhan, Hubei, China

<sup>10</sup>Northwestern University Feinberg School of Medicine, Chicago, Illinois, USA

<sup>11</sup>Abbott Molecular Inc, Des Plaines, Illinois, USA

**Contributors** BW and XW conceived and designed the study. JH, FD, YH, and XX performed the experiments and analyzed the data, FC, JH, QX, MD, and XL provided the clinical samples. TL, WL, QG, SC, XH, PZ, GL, YL Provide technical support. HJ wrote the paper with feedback provided by all the authors. XW, BW, XY, GX, and DG reviewed and revised the manuscript.

**Funding** This research work was supported by the National Natural Science Foundation of China (82072797 to BW; 81772676 to XW; 82002654 to FD). Key projects from Tianjin Education Commission (2020ZD13 to XW). Natural Science Foundation of Tianjin City (18JCJQJC48200 to XW). Natural Science Foundation of Hubei (2020CFB671). China Postdoctoral Science Foundation (2022T150474 to FD). We shall extend our thanks to members of Wu lab and Yu lab for the helpful discussion.

**Competing interests** None declared.

**Patient consent for publication** Not applicable.

**Ethics approval** Human subject-related research was approved, according to the Declaration of Helsinki, by the Institutional Review Board at Tongji Hospital, with informed consent. The collection and usage of patient tumor tissue samples were approved by the Research Ethics Committee of Tongji Hospital, Tongji Medical College, Huazhong University of Science and Technology (serial no.TJ-IBR20181111). The animal study protocol was approved by the Institutional Animal Use and Care Committee at Tianjin Medical University. This study was approved by The Research Ethics Committee of Tianjin Medical University (TMUaMEC-2017009).

**Provenance and peer review** Not commissioned; externally peer reviewed.

**Data availability statement** No data are available.

**Supplemental material** This content has been supplied by the author(s). It has not been vetted by BMJ Publishing Group Limited (BMJ) and may not have been peer-reviewed. Any opinions or recommendations discussed are solely those of the author(s) and are not endorsed by BMJ. BMJ disclaims all liability and responsibility arising from any reliance placed on the content. Where the content includes any translated material, BMJ does not warrant the accuracy and reliability of the translations (including but not limited to local regulations, clinical guidelines, terminology, drug names and drug dosages), and is not responsible for any error and/or omissions arising from translation and adaptation or otherwise.

**Open access** This is an open access article distributed in accordance with the Creative Commons Attribution Non Commercial (CC BY-NC 4.0) license, which permits others to distribute, remix, adapt, build upon this work non-commercially, and license their derivative works on different terms, provided the original work is properly cited, appropriate credit is given, any changes made indicated, and the use is non-commercial. See <http://creativecommons.org/licenses/by-nc/4.0/>.

#### ORCID iD

Feng Dong <http://orcid.org/0000-0003-1807-561X>

#### REFERENCES

- GBD 2016 Brain and Other CNS Cancer Collaborators. Global, regional, and national burden of brain and other CNS cancer, 1990–2016: a systematic analysis for the global burden of disease study 2016. *Lancet Neurol* 2019;18:376–93.
- Stupp R, Taillibert S, Kanner A, et al. Effect of tumor-treating fields plus maintenance temozolomide vs maintenance temozolomide alone on survival in patients with glioblastoma: a randomized clinical trial. *JAMA* 2017;318:2306–16.
- Venkatesh HS, Tam LT, Woo PJ, et al. Targeting neuronal activity-regulated neuroligin-3 dependency in high-grade glioma. *Nature* 2017;549:533–7.
- Woroniecka K, Chongsathidkiet P, Rhodin K, et al. T-cell exhaustion signatures vary with tumor type and are severe in glioblastoma. *Clin Cancer Res* 2018;24:4175–86.
- Hu J, Xiao Q, Dong M, et al. Glioblastoma immunotherapy targeting the innate immune checkpoint CD47–SIRP $\alpha$  axis. *Front Immunol* 2020;11:593219.
- Cassetta L, Pollard JW. Targeting macrophages: therapeutic approaches in cancer. *Nat Rev Drug Discov* 2018;17:887–904.
- Chen Q, Jin J, Huang X, et al. Emp3 mediates glioblastoma-associated macrophage infiltration to drive T cell exclusion. *J Exp Clin Cancer Res* 2021;40:160.
- Klichinsky M, Ruella M, Shestova O, et al. Human chimeric antigen receptor macrophages for cancer immunotherapy. *Nat Biotechnol* 2020;38:947–53.
- Stafford JH, Hirai T, Deng L, et al. Colony stimulating factor 1 receptor inhibition delays recurrence of glioblastoma after radiation by altering myeloid cell recruitment and polarization. *Neuro Oncol* 2016;18:797–806.
- Pyonteck SM, Akkari L, Schuhmacher AJ, et al. CSF-1R inhibition alters macrophage polarization and blocks glioma progression. *Nat Med* 2013;19:1264–72.
- Veillette A, Chen J. SIRP $\alpha$ –CD47 immune checkpoint blockade in anticancer therapy. *Trends Immunol* 2018;39:173–84.
- Alvey CM, Spinler KR, Irianto J, et al. SIRP $\alpha$ -inhibited, marrow-derived macrophages engorge, accumulate, and differentiate in antibody-targeted regression of solid tumors. *Curr Biol* 2017;27:2065–77.
- Guo D, Nilsson J, Haapasalo H, et al. Perinuclear leucine-rich repeats and immunoglobulin-like domain proteins (LRIG1–3) as prognostic indicators in astrocytic tumors. *Acta Neuropathol* 2006;111:238–46.
- Mao F, Wang B, Xiao Q, et al. LRIG proteins in glioma: functional roles, molecular mechanisms, and potential clinical implications. *J Neurol Sci* 2017;383:56–60.
- Dong M, Xiao Q, Hu J, et al. Targeting LRIG2 overcomes resistance to EGFR inhibitor in glioblastoma by modulating GAS6/AXL/SRC signaling. *Cancer Gene Ther* 2020;27:878–97.
- Aguilera TA, Giaccia AJ. Molecular pathways: oncologic pathways and their role in T-cell exclusion and immune Evasion–A new role for the Axl receptor tyrosine kinase. *Clin Cancer Res* 2017;23:2928–33.
- Agliardi G, Liuzzi AR, Hotblack A, et al. Intratumoral IL-12 delivery empowers CAR-T cell immunotherapy in a pre-clinical model of glioblastoma. *Nat Commun* 2021;12:444.
- Song X, Shao Y, Jiang T, et al. Radiotherapy upregulates programmed death ligand-1 through the pathways downstream of epidermal growth factor receptor in glioma. *EBioMedicine* 2018;28:105–13.
- Sadahiro H, Kang K-D, Gibson JT, et al. Activation of the receptor tyrosine kinase AXL regulates the immune microenvironment in glioblastoma. *Cancer Res* 2018;78:3002–13.
- Rondahl V, Holmlund C, Karlsson T, et al. Lig2-deficient mice are protected against PDGFB-induced glioma. *PLoS One* 2013;8:e73635.
- Neirinckx V, Hau A-C, Schuster A, et al. The soluble form of pan-RTK inhibitor and tumor suppressor LRIG1 mediates downregulation of Axl through direct protein-protein interaction in glioblastoma. *Neurooncol Adv* 2019;1:vdz024.
- Xiao Q, Tan Y, Guo Y, et al. Soluble LRIG2 ectodomain is released from glioblastoma cells and promotes the proliferation and inhibits the apoptosis of glioblastoma cells in vitro and in vivo in a similar manner to the full-length LRIG2. *PLoS One* 2014;9:e111419.
- Cheng F, Zhang P, Xiao Q, et al. The prognostic and therapeutic potential of Lig3 and soluble Lig3 in glioblastoma. *Front Oncol* 2019;9:447.
- Johansson M, Oudin A, Tiemann K, et al. The soluble form of the tumor suppressor LRIG1 potently inhibits in vivo glioma growth irrespective of EGF receptor status. *Neuro Oncol* 2013;15:1200–11.
- Bowman RL, Wang Q, Carro A, et al. GlioVis data portal for visualization and analysis of brain tumor expression datasets. *Neuro Oncol* 2017;19:139–41.
- Darmanis S, Sloan SA, Croote D, et al. Single-Cell RNA-seq analysis of infiltrating neoplastic cells at the migrating front of human glioblastoma. *Cell Rep* 2017;21:1399–410.
- Dong F, Li Q, Yang C, et al. PRMT2 links histone H3R8 asymmetric dimethylation to oncogenic activation and tumorigenesis of glioblastoma. *Nat Commun* 2018;9:4552.
- Liu Y, Chen K, Wang C, et al. Cell surface receptor Fpr2 promotes antitumor host defense by limiting M2 polarization of macrophages. *Cancer Res* 2013;73:550–60.
- Wu X, Bekker-Jensen IH, Christensen J, et al. Tumor suppressor ASXL1 is essential for the activation of INK4B expression in response to oncogene activity and anti-proliferative signals. *Cell Res* 2015;25:1205–18.

- 30 Barkal AA, Brewer RE, Markovic M, *et al.* CD24 signalling through macrophage Siglec-10 is a target for cancer immunotherapy. *Nature* 2019;572:392–6.
- 31 Gholamin S, Mitra SS, Feroze AH, *et al.* Disrupting the CD47-SIRP $\alpha$  anti-phagocytic axis by a humanized anti-CD47 antibody is an efficacious treatment for malignant pediatric brain tumors. *Sci Transl Med* 2017;9. doi:10.1126/scitranslmed.aaf2968. [Epub ahead of print: 15 03 2017].
- 32 Woolf Z, Swanson MEV, Smyth LC, *et al.* Single-cell image analysis reveals a protective role for microglia in glioblastoma. *Neurooncol Adv* 2021;3:vdab031.
- 33 Liu X, Pu Y, Cron K, *et al.* CD47 blockade triggers T cell-mediated destruction of immunogenic tumors. *Nat Med* 2015;21:1209–15.
- 34 Majeti R, Chao MP, Alizadeh AA, *et al.* CD47 is an adverse prognostic factor and therapeutic antibody target on human acute myeloid leukemia stem cells. *Cell* 2009;138:286–99.
- 35 Hou P-P, Luo L-J, Chen H-Z, *et al.* Ectosomal PKM2 promotes HCC by inducing macrophage differentiation and remodeling the tumor microenvironment. *Mol Cell* 2020;78:1192–206.
- 36 Mathew LK, Skuli N, Mucaj V, *et al.* miR-218 opposes a critical RTK-HIF pathway in mesenchymal glioblastoma. *Proc Natl Acad Sci U S A* 2014;111:291–6.
- 37 Cui L, Chen S-Y, Lerbs T, *et al.* Activation of Jun in fibroblasts promotes pro-fibrotic programme and modulates protective immunity. *Nat Commun* 2020;11:2795.
- 38 Ghosh D, Funk CC, Caballero J, *et al.* A cell-surface membrane protein signature for glioblastoma. *Cell Syst* 2017;4:516–29.
- 39 Yi W, Holmlund C, Nilsson J, *et al.* Paracrine regulation of growth factor signaling by shed leucine-rich repeats and immunoglobulin-like domains 1. *Exp Cell Res* 2011;317:504–12.
- 40 Saad MI, Rose-John S, Jenkins BJ. ADAM17: an emerging therapeutic target for lung cancer. *Cancers* 2019;11. doi:10.3390/cancers11091218. [Epub ahead of print: 21 08 2019].
- 41 Cioffi M, Trabulo S, Hidalgo M, *et al.* Inhibition of CD47 effectively targets pancreatic cancer stem cells via dual mechanisms. *Clin Cancer Res* 2015;21:2325–37.
- 42 von Roemeling CA, Wang Y, Qie Y, *et al.* Therapeutic modulation of phagocytosis in glioblastoma can activate both innate and adaptive antitumour immunity. *Nat Commun* 2020;11:1508.